

Heat-based circuits using quantum rectification

Kasper Poulsen* and Nikolaj T. Zinner†

Department of Physics and Astronomy, Aarhus University, Ny Munkegade 120, 8000 Aarhus C, Denmark

With increased power consumption of modern computer components, a heat-based computer has become ever more relevant due to a lower power expense to process logic bits of information. In a heat-based computer, computations are performed by driving heat currents through a circuit using a temperature difference. Utilizing harmonic oscillators and three-level quantum rectifiers as base components, we study three different heat-based circuits: a series configuration of diodes, a parallel configuration of diodes, and a diode bridge rectifier. We demonstrate the required functionality of each circuit for use as heat-based analogues of standard electronic components. Furthermore, the diode bridge rectifier is found to give consistent output bias independent of the input bias thus rectifying the input. Our results prove the theoretical feasibility of combining heat current components into heat-based circuits. The three circuits should be realizable using several of the current quantum technology platforms.

I. INTRODUCTION

As minituration of classical transistors become increasingly difficult, the effort to keep Moore's law alive has led to increased energy consumption of computer components [1]. It is hoped that not only charge but also alternative information carriers such as magnetic (spin) [2–4] and thermal (phonon) [5, 6] currents can be leveraged in future technologies. Thermal currents are driven by subjecting a heat circuit to a temperature difference, and a heat-based computer could, therefore, be powered by excess heat making it an especially promising platform through its low energy consumption.

With the development of quantum technologies, the understanding of heat transport necessary for a heat-based computer has increased substantially. This includes theoretical proposals of minimal engines [7–9], entanglement engines [10], and various versions of Maxwell's demon [11–13]. Additionally, experiments have proven the feasibility of heat control in systems such as Maxwell's demon [14, 15], diodes [16], and heat valves [17].

A functioning heat based computer requires a toolbox of versatile components which can be used to control the heat flow inside the computer. Many such components, such as transistors [18–20] and diodes [21–27], have been proposed. Most proposals study the component exposed directly to a temperature bias i.e. a transistor or diode coupled directly to thermal baths at either end. However, to achieve a heat-based computer, more complex circuits composed of multiple components are required. Many of these components rely on this proximity to the thermal baths, and therefore, they can not trivially be used in larger circuits. One popular circuit in classical electronics is the full wave bridge rectifier, which is a bridge consisting of four diodes [28]. The purpose of the full wave bridge rectifier is to convert an alternating current into a direct current such that the output voltage is of the same sign independent of the input voltage.

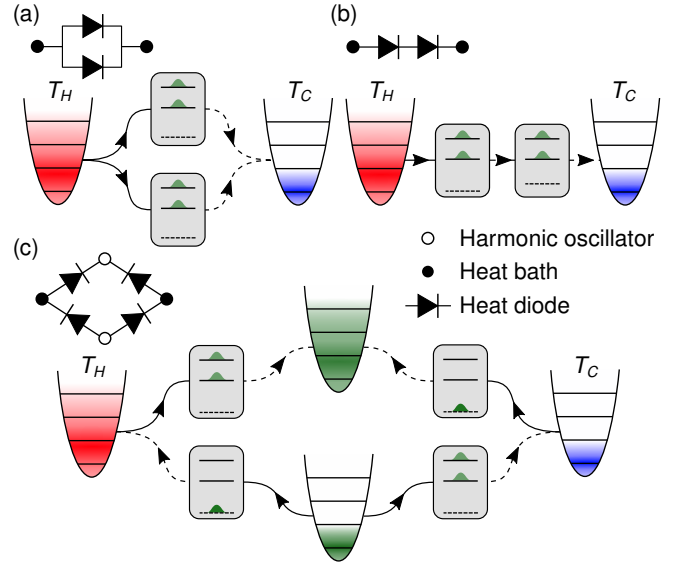


Figure 1. Schematic of the three different circuits studied: (a) parallel configuration of diodes, (b) Series configuration of diodes, and (c) diode bridge rectifier. The circuits are shown both using a level diagram and more traditional circuit pictograms.

Here, we study three different heat-based circuits as seen in Fig. 1: a series configuration of diodes, a parallel configuration of diodes, and a diode bridge rectifier. All three circuits are comprised of harmonic oscillators and three-level quantum systems that can be operated as quantum rectifiers or diodes [21]. The general circuit setup is a heat source and a heat drain each coupled to a harmonic oscillator of equal frequency. These harmonic oscillators act as input and output filters setting the scale of the energy quanta of the heat current. The circuits are built up of components connecting the input and output harmonic oscillators. We show that the functionality of the components have added complexity when compared to a single component circuit. However, the functionality of the components is generally persistent across all three circuits, enabling their use as a heat-based alternative to their standard electronics counterparts.

* poulsen@phys.au.dk

† zinner@phys.au.dk

II. RESULTS

The Hamiltonian for all three of the circuits studied here takes the form

$$\hat{H} = \omega(\hat{a}_L^\dagger \hat{a}_L + \hat{a}_R^\dagger \hat{a}_R) + \hat{H}_{\text{Circuit}},$$

where \hat{a}_L and \hat{a}_R are ladder operators for the left (L) and right (R) harmonic oscillators, respectively. \hat{H}_{Circuit} is the Hamiltonian for the circuit connecting L and R. We are using units where $\hbar = k_B = 1$. To drive a heat current through the circuit L and R are coupled to thermal baths through the Lindblad master equation [29, 30]

$$\frac{d\hat{\rho}}{dt} = -i[\hat{H}, \hat{\rho}] + \mathcal{D}_L[\hat{\rho}] + \mathcal{D}_R[\hat{\rho}], \quad (1)$$

where $[\bullet, \bullet]$ is the commutator, $\mathcal{L}[\hat{\rho}]$ is the Lindblad superoperator, and $\mathcal{D}_{L(R)}[\hat{\rho}]$ is a dissipative term describing the action of the left (right) bath

$$\mathcal{D}_{L(R)}[\hat{\rho}] = \Gamma(n_{L(R)} + 1)\mathcal{M}[\hat{a}_{L(R)}, \hat{\rho}] + \Gamma n_{L(R)}\mathcal{M}[\hat{a}_{L(R)}^\dagger, \hat{\rho}],$$

where $\mathcal{M}[\hat{A}, \hat{\rho}] = \hat{A}\hat{\rho}\hat{A}^\dagger - \{\hat{A}^\dagger\hat{A}, \hat{\rho}\}/2$, and $\{\bullet, \bullet\}$ is the anti-commutator. Γ is the coupling strength between the baths and harmonic oscillators and $n_{L(R)} = (e^{\omega/T_{L(R)}} - 1)^{-1}$ is the mean number of excitations in the left (right) harmonic oscillator in the absence of the circuit. The harmonic oscillators act as filters of frequency ω between the baths and the circuit. After sufficient time the system will reach steady state. See the methods section for information on when the system is considered to have reached steady state. It is the properties of the steady state that we will focus on. The circuit connecting L and R is comprised of Harmonic oscillators and quantum rectifiers. The quantum rectifier used is a qutrit in the form of an anharmonic oscillator truncated to the three lowest states [21], however, any three level system could be used. The Hamiltonian for the qutrit diode α connecting two harmonic oscillators A and B is

$$\begin{aligned} \hat{H}_{A \rightarrow B}^\alpha = & \omega \hat{a}_\alpha^\dagger \hat{a}_\alpha - \delta\omega_\alpha |0_\alpha\rangle\langle 0_\alpha| + \\ & + J_\alpha(t)(\hat{a}_A \hat{a}_\alpha^\dagger + \hat{a}_A^\dagger \hat{a}_\alpha) + J(\hat{a}_\alpha \hat{a}_B^\dagger + \hat{a}_\alpha^\dagger \hat{a}_B), \end{aligned} \quad (2)$$

where $\hat{a}_\alpha = |0_\alpha\rangle\langle 1_\alpha| + \sqrt{2}|1_\alpha\rangle\langle 2_\alpha|$. $|0_\alpha\rangle$, $|1_\alpha\rangle$, and $|2_\alpha\rangle$ are the three qutrit states. The two excited states are resonant with the harmonic oscillators with energy difference ω . The ground state is a dark state of B due to the anharmonicity $\delta\omega_\alpha$. The coupling to A is time-dependent with coupling strength $J_\alpha(t) = J + J' \cos(\delta\omega_\alpha t)$. In the limit $\omega, \delta\omega \gg J, J'$, the number of excitations exchanged between the left (right) harmonic oscillator and left (right) bath per unit of time is

$$\mathcal{J}_{L(R)} = \Gamma n_{L(R)} \langle \hat{a}_{L(R)} \hat{a}_{L(R)}^\dagger \rangle_{\text{ss}} - \Gamma(n_{L(R)} + 1) \langle \hat{a}_{L(R)}^\dagger \hat{a}_{L(R)} \rangle_{\text{ss}}, \quad (3)$$

where $\langle \bullet \rangle_{\text{ss}} = \text{tr}\{\bullet \hat{\rho}_{\text{ss}}\}$ is the steady state expectation value, and $\text{tr}\{\bullet\}$ is the trace over the entire Hilbert space. This is the excitation current whereas the heat current is given by $\omega \mathcal{J}_{L(R)}$. We will focus on the limit $\Gamma \gg J$ where L and R are assumed to be in a thermal state due to the strong coupling to the baths.

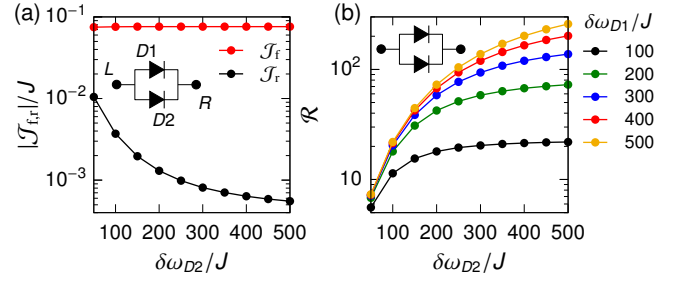


Figure 2. (a) Forward and reverse bias current as a function of the anharmonicity $\delta\omega_{D2}$ for a parallel configuration of diodes. (b) Rectification as a function of $\delta\omega_{D2}$ for a parallel configuration of diodes.

This is the Markovian limit, and the two harmonic oscillators can be traced away thus lowering the degrees of freedom that has to be simulated, for further details see [13, 30, 31]. Unless otherwise stated, we use $\delta\omega_\alpha = 300J$, $J' = 0.5J$, and $\Gamma = 10J$. The simplest circuit of one diode is

$$\hat{H}_{\text{Circuit}} = \hat{H}_{L \rightarrow R}^{D1}, \quad (4)$$

which has been studied in [21]. However, the functionality can be summarized in two parts. For $n_L > n_R$, excitations can propagate via transitions like

$$\text{Forward: } |1_L 1_{D1} 0_R\rangle \leftrightarrow |0_L 2_{D1} 0_R\rangle \leftrightarrow |0_L 1_{D1} 1_R\rangle.$$

For $n_L < n_R$, the qutrit is trapped in the dark state $|0_T\rangle$ through the transition

$$\text{Reverse: } |0_L 1_{D1} 0_R\rangle \leftrightarrow |1_L 0_{D1} 0_R\rangle \rightarrow |0_L 0_{D1} 0_R\rangle.$$

Since $|0_{D1}\rangle$ is a dark state of the right bath it will block transport in reverse bias. Here we will look at both a parallel and series configuration of diodes as well as a heat-based diode bridge rectifier.

A. Parallel configuration of diodes

First, we will study the rectification of a parallel configuration of qutrit diodes as seen in Fig. 1(a). The Hamiltonian for the parallel configuration is

$$\hat{H}_{\text{Circuit}} = \sum_{\alpha \in \{D1, D2\}} \hat{H}_{L \rightarrow R}^\alpha.$$

Invoking the Markov approximation, the master equation for the density matrix of just the two qutrits becomes

$$\frac{d\hat{\rho}}{dt} = \sum_{\alpha=D1, D2} \sum_{A, B \in \mathcal{H}_\alpha} [\Gamma_{A \rightarrow B}^L + \Gamma_{A \rightarrow B}^R] \mathcal{M}[|B\rangle\langle A|, \hat{\rho}], \quad (5)$$

where $\mathcal{H}_\alpha = \{0_\alpha, 1_\alpha, 2_\alpha\}$ and

$$\Gamma_{0_\alpha \rightarrow 1_\alpha}^L = \frac{n_L J'^2}{\Gamma} + \frac{n_L J^2 \Gamma}{\delta\omega_\alpha^2 + \Gamma^2/4}, \quad \Gamma_{1_\alpha \rightarrow 2_\alpha}^L = \frac{8n_L J^2}{\Gamma}, \quad (6a)$$

$$\Gamma_{1_\alpha \rightarrow 0_\alpha}^L = \frac{(1+n_L)J'^2}{\Gamma} + \frac{(1+n_L)J^2 \Gamma}{\delta\omega_\alpha^2 + \Gamma^2/4}, \quad \Gamma_{2_\alpha \rightarrow 1_\alpha}^L = \frac{8(1+n_L)J^2}{\Gamma}, \quad (6b)$$

$$\Gamma_{0_\alpha \rightarrow 1_\alpha}^R = \frac{n_R J^2 \Gamma}{\delta\omega_\alpha^2 + \Gamma^2/4}, \quad \Gamma_{1_\alpha \rightarrow 2_\alpha}^R = \frac{8n_R J^2}{\Gamma}, \quad (6c)$$

$$\Gamma_{1_\alpha \rightarrow 0_\alpha}^R = \frac{(1+n_R)J^2 \Gamma}{\delta\omega_\alpha^2 + \Gamma^2/4}, \quad \Gamma_{2_\alpha \rightarrow 1_\alpha}^R = \frac{8(1+n_R)J^2}{\Gamma}, \quad (6d)$$

for $\alpha \in \{D1, D2\}$. All other rates are zero. The right bath rates $\Gamma_{A \rightarrow B}^R$ are similar to the left bath rates $\Gamma_{A \rightarrow B}^L$ without the term containing J' . Therefore, these rates will be useful whenever a diode is coupled to either the left or right harmonic oscillator. By forward bias, we denote the case where $n_L = 0.5$ and $n_R = 0$, and heat flows from left to right. By reverse bias, we denote the case where $n_L = 0$ and $n_R = 0.5$, and heat flows from right to left. We define the forward bias excitation current to be $\mathcal{J}_f = -\mathcal{J}_R$, while the reverse bias excitation current is $\mathcal{J}_r = \mathcal{J}_L$. The quality of the diode is quantified using the rectification

$$\mathcal{R} = -\frac{\mathcal{J}_f}{\mathcal{J}_r},$$

which tends to infinity for a perfect diode. Since L and R have been traced away, Eq. (3) is not directly applicable. Instead, the number of excitations decaying to the bath is calculated directly,

$$\mathcal{J}_f = \sum_{\alpha=D1, D2} \left[\langle 1_\alpha | \hat{\rho}_{ss,f} | 1_\alpha \rangle \Gamma_{1_\alpha \rightarrow 0_\alpha}^R + \langle 2_\alpha | \hat{\rho}_{ss,f} | 2_\alpha \rangle \Gamma_{2_\alpha \rightarrow 1_\alpha}^R \right],$$

$$\mathcal{J}_r = - \sum_{\alpha=D1, D2} \left[\langle 1_\alpha | \hat{\rho}_{ss,r} | 1_\alpha \rangle \Gamma_{1_\alpha \rightarrow 0_\alpha}^L + \langle 2_\alpha | \hat{\rho}_{ss,r} | 2_\alpha \rangle \Gamma_{2_\alpha \rightarrow 1_\alpha}^L \right].$$

The forward and reverse bias currents can be seen in Fig. 2(a). The reverse bias current is clearly suppressed for large $\delta\omega_{D2}$ as expected. In Fig. 2(b), the rectification for different values of $\delta\omega_{D1}$ and $\delta\omega_{D2}$ is plotted. These results look similar to the ones presented in [21]. In fact, Eq. (5) does not couple the two qutrits, and the system simplifies to two decoupled qutrit diodes. For $\delta\omega_{D1} = 100J$, the rectification is smallest, since the rectification is limited by the worst of the two diodes.

B. Series configuration of diodes

Next, we study the rectification of a series configuration of qutrit diodes as seen in Fig. 1(b). The most obvious series configuration consists of an extra harmonic oscillator added between two diodes. However, we will study a more compact

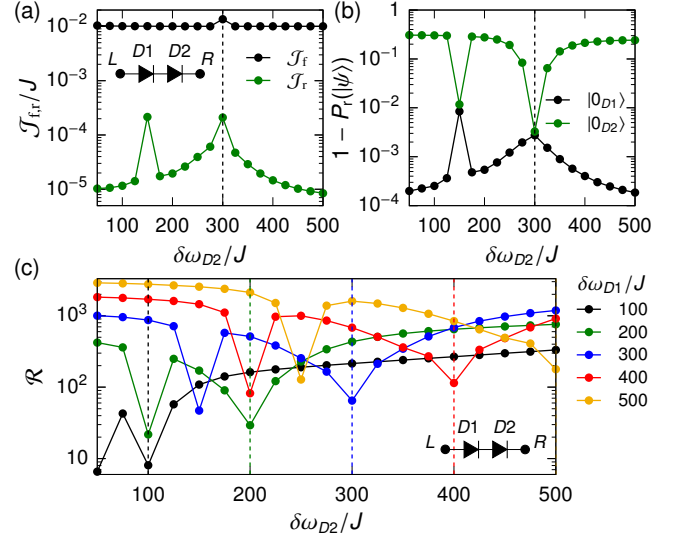


Figure 3. (a) Forward and reverse bias current as a function of the anharmonicity $\delta\omega_{D2}$ for a series configuration of diodes. (b) Ground-state population of the two qutrits as a function of $\delta\omega_{D2}$ for a series configuration of diodes. (c) Rectification as a function of the anharmonicity $\delta\omega_{D2}$ for a series configuration of diodes. The dashed lines correspond to $\delta\omega_{D1} = \delta\omega_{D2}$.

version of just two diodes in series. The Hamiltonian of this series configuration is

$$\hat{H}_{\text{Circuit}} = \hat{H}_{L \rightarrow D2}^{D1} + \hat{H}_{D1 \rightarrow R}^{D2},$$

where the diode Hamiltonians have to be modified to accommodate the compact circuit

$$\hat{H}_{L \rightarrow D2}^{D1} = \omega \hat{a}_{D1}^\dagger \hat{a}_{D1} - \delta\omega_{D1} |0_{D1}\rangle \langle 0_{D1}| + J_{D1}(t) (\hat{a}_L \hat{a}_{D1}^\dagger + \hat{a}_L^\dagger \hat{a}_{D1}),$$

$$\hat{H}_{D1 \rightarrow R}^{D2} = \omega \hat{a}_{D2}^\dagger \hat{a}_{D2} - \delta\omega_{D2} |0_{D2}\rangle \langle 0_{D2}| + J_{D2}(t) (\hat{a}_{D1} \hat{a}_{D2}^\dagger + \hat{a}_{D1}^\dagger \hat{a}_{D2}) + J (\hat{a}_{D2} \hat{a}_R^\dagger + \hat{a}_{D2}^\dagger \hat{a}_R).$$

Since $\Gamma \gg J$, we can trace L and R away resulting in a master equation for just the two qutrits similar to the previous section.

$$\frac{d\hat{\rho}}{dt} = -i[\hat{H}_{\text{Circuit}} - \hat{H}_{SB}, \hat{\rho}] + \sum_{A,B \in \mathcal{H}_{D1}} \Gamma_{A \rightarrow B}^L \mathcal{M}[|B\rangle\langle A|, \hat{\rho}] + \sum_{A,B \in \mathcal{H}_{D2}} \Gamma_{A \rightarrow B}^R \mathcal{M}[|B\rangle\langle A|, \hat{\rho}], \quad (7)$$

where \hat{H}_{SB} is the new system bath coupling which is now included in the dissipative terms

$$\hat{H}_{SB} = J_{D1}(t) (\hat{a}_L \hat{a}_{D1}^\dagger + \hat{a}_L^\dagger \hat{a}_{D1}) + J (\hat{a}_{D2} \hat{a}_R^\dagger + \hat{a}_{D2}^\dagger \hat{a}_R).$$

The transport is quantified using the excitation current which for this circuit becomes

$$\mathcal{J}_f = \langle 1_{D2} | \hat{\rho}_{ss,f} | 1_{D2} \rangle \Gamma_{1_{D2} \rightarrow 0_{D2}}^R + \langle 2_{D2} | \hat{\rho}_{ss,f} | 2_{D2} \rangle \Gamma_{2_{D2} \rightarrow 1_{D2}}^R,$$

$$\mathcal{J}_r = - \left[\langle 1_{D1} | \hat{\rho}_{ss,r} | 1_{D1} \rangle \Gamma_{1_{D1} \rightarrow 0_{D1}}^L + \langle 2_{D1} | \hat{\rho}_{ss,r} | 2_{D1} \rangle \Gamma_{2_{D1} \rightarrow 1_{D1}}^L \right].$$

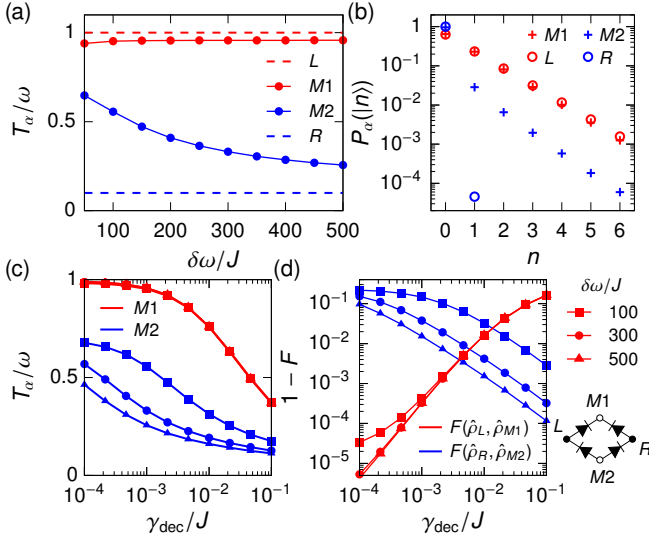


Figure 4. (a) Effective temperature of the harmonic oscillators as a function of the qutrit anharmonicity for the bridge rectifier. (b) Populations of the harmonic oscillators $P_\alpha(n)$ for $\alpha = L, M1, M2, R$ for the bridge rectifier. (c) Effective temperature of the middle harmonic oscillators as a function of the decoherence rate γ_{dec} . (d) Fidelities between the states of the harmonic oscillators pairwise as a function of the decoherence rate γ_{dec} .

In Fig. 3(a), the forward and reverse bias currents are plotted as a function of $\delta\omega_{D2}$. The dashed line denotes $\delta\omega_{D1} = \delta\omega_{D2}$. The reverse bias current has two peaks; a narrow peak at $\delta\omega_{D2} = \delta\omega_{D1}/2$ and a wider peak at $\delta\omega_{D2} = \delta\omega_{D1}$. To further investigate the drop in diode functionality at these two values, we plot the reverse-bias ground-state population of the two qutrits in Fig. 3(b). We know from Ref. [21] that a current is prevented due to the ground state being populated. Therefore, Fig. 3(b) shows that the first qutrit (D1) is predominantly responsible for the large rectification. However, at the two special points $\delta\omega_{D2} = \delta\omega_{D1}/2$ and $\delta\omega_{D2} = \delta\omega_{D1}$ the populations are similar and the rectification is due to both qutrits. In Fig. 3(c), the rectification is plotted for the series configuration of qutrit diodes. Rectification factors in the excess of 10^3 are achieved, and the drops in rectification for $\delta\omega_{D2} = \delta\omega_{D1}/2$ and $\delta\omega_{D2} = \delta\omega_{D1}$ are still seen. So even though only one qutrit contributes to the rectification through ground state population, the overall rectification factors are still larger than for the parallel configuration. This is possible since the second qutrit (D2) can act as a filter making the effective interaction between the first qutrit (D1) and the right bath smaller.

C. Diode Bridge Rectifier

The circuit for the bridge rectifier consists of four diodes and two additional harmonic oscillators as seen in Fig. 1(c). If the qutrit diodes function as intended, the bias of the top and bottom harmonic oscillators will remain the same independent of the bias of the left and right harmonic oscillators. Since the circuit is horizontally symmetric, we can assume $T_L \geq T_R$.

The Hamiltonian becomes

$$\hat{H}_{\text{Circuit}} = \hat{H}_{L \rightarrow M1}^{D1} + \hat{H}_{R \rightarrow M1}^{D2} + \hat{H}_{M2 \rightarrow L}^{D3} + \hat{H}_{M2 \rightarrow R}^{D4} + \omega(\hat{a}_{M1}^\dagger \hat{a}_{M1} + \hat{a}_{M2}^\dagger \hat{a}_{M2}),$$

where \hat{a}_{M1} and \hat{a}_{M2} are annihilation operators for the upper and lower harmonic oscillator, respectively. We choose all anharmonicities the same, $\delta\omega$. The effective master equation becomes

$$\frac{d\hat{\rho}}{dt} = -i[\hat{H}_{\text{Circuit}} - \hat{H}_{SB}, \hat{\rho}] + \gamma_{\text{dec}} \sum_{\alpha} (\mathcal{M}[\hat{a}_{\alpha}, \hat{\rho}] + \mathcal{M}[\hat{a}_{\alpha}^\dagger \hat{a}_{\alpha}, \hat{\rho}]) + \mathcal{K}_L^{D1}[\hat{\rho}] + \mathcal{K}_R^{D2}[\hat{\rho}] + \mathcal{K}_L^{D3}[\hat{\rho}] + \mathcal{K}_R^{D4}[\hat{\rho}], \quad (8)$$

where \hat{H}_{SB} is the new system bath coupling which is now included in the dissipative terms

$$\hat{H}_{SB} = J_{D1}(t)(\hat{a}_L \hat{a}_{D1}^\dagger + \hat{a}_L^\dagger \hat{a}_{D1}) + J_{D2}(t)(\hat{a}_{D2} \hat{a}_R^\dagger + \hat{a}_{D2}^\dagger \hat{a}_R) + J(\hat{a}_L \hat{a}_{D3}^\dagger + \hat{a}_L^\dagger \hat{a}_{D3}) + J(\hat{a}_{D4} \hat{a}_R^\dagger + \hat{a}_{D4}^\dagger \hat{a}_R). \quad (9)$$

The constant γ_{dec} is the decoherence rate, which unless otherwise stated, is set to $\gamma_{\text{dec}} = 10^{-3}J$. The sum over α in Eq. (8) is carried out for $\alpha \in \{D1, M1, D2, D3, M2, D4\}$. The last four terms describe the effective interaction of the baths with the four qutrits, e.g., $\mathcal{K}_L^{D1}[\hat{\rho}] = \sum_{A,B \in \mathcal{H}_{D1}} \Gamma_{A \rightarrow B}^L \mathcal{M}[|B\rangle\langle A|, \hat{\rho}]$. To quantify the functionality of the bridge rectifier, we use the temperature of the two harmonic oscillators M1 and M2. Since the states of M1 and M2 are not necessarily a thermal state, we use the effective temperature

$$T_\alpha/\omega = [\ln(\langle \hat{n}_\alpha \rangle_{\text{ss}} + 1) - \ln \langle \hat{n}_\alpha \rangle_{\text{ss}}]^{-1}, \quad (10)$$

which is the temperature of a thermal state with the same occupation number $\langle \hat{n}_\alpha \rangle_{\text{ss}}$ as the harmonic oscillators. In Fig. 4(a), the effective temperature of the four harmonic oscillators is plotted as a function of the diode quality parametrized through $\delta\omega$. This is compared to the temperatures of the left and right baths, $T_L = \omega$ and $T_R = 0.1\omega$ plotted with dashed lines. A perfect rectifier bridge would result in:

$$T_L \simeq T_{M1} \quad \text{and} \quad T_R \simeq T_{M2}.$$

From Fig. 4(a), we see that T_{M1} quickly approaches T_L . The discrepancy between T_{M1} and T_L for large $\delta\omega$ is mainly due to decay through γ_{dec} . In Fig. 4(b), the populations of the harmonic oscillator states are plotted. The populations for a thermal state with mean excitation number $\langle \hat{n}_\alpha \rangle_{\text{ss}}$ is

$$P(n) = \frac{\langle \hat{n}_\alpha \rangle_{\text{ss}}^n}{[1 + \langle \hat{n}_\alpha \rangle_{\text{ss}}]^{n+1}}, \quad (11)$$

which is the population of L and R within the Markov approximation. Since Fig. 4(b) is a log plot, thermal states will be points along a line. Harmonic oscillator M1 does indeed overlap with the thermal state of L. Harmonic oscillator M2 is clearly cold, but the state is not a thermal state. For M1 to get cold in the long time limit, diode D3 needs to close i.e. be driven into the ground state $|0_{D3}\rangle$. This can either be done

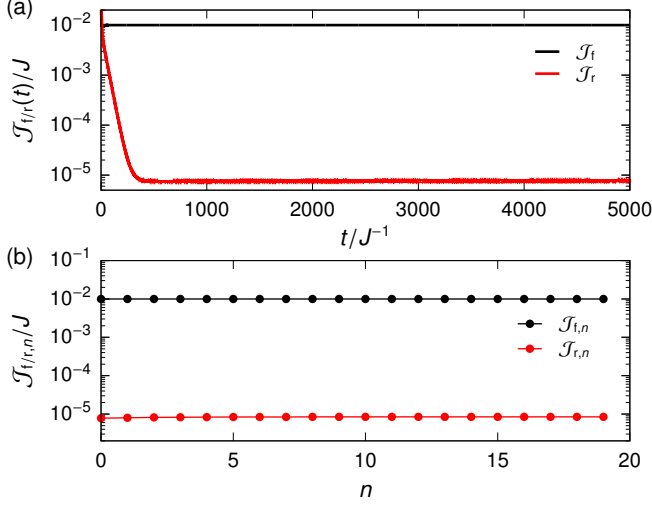


Figure 5. (a) Forward and reverse bias currents as a function of time. (b) Average currents in both forward and reverse bias as a function of the integer n .

by the cold right bath or through the decoherence rate γ_{dec} . To test the importance of γ_{dec} , we plot the effective temperatures as a function of γ_{dec} for three different values of $\delta\omega$ in Fig. 4(c). Clearly, decay through γ_{dec} is important for M2 to be cold. However, for larger γ_{dec} , the effective temperature of M1 decreases due to decay. Since the states of M1 and M2 are not necessarily thermal, it is interesting to look at the fidelity between the relevant pairs of states. The fidelity between two density matrices is

$$F(\hat{\rho}_1, \hat{\rho}_2) = \left[\text{tr} \sqrt{\sqrt{\hat{\rho}_1} \hat{\rho}_2 \sqrt{\hat{\rho}_1}} \right]^2. \quad (12)$$

The density matrix for $\alpha \in \{L, M1, M2, R\}$ is $\hat{\rho}_\alpha = \text{tr}_{S \setminus \alpha} \{\hat{\rho}\}$ where the trace is over the entire system except α . The fidelities between two pairs of states $F(\hat{\rho}_L, \hat{\rho}_{M1})$ and $F(\hat{\rho}_R, \hat{\rho}_{M2})$ are plotted in Fig. 4(d). The fidelity between the state of M1 and L becomes smaller for larger γ_{dec} , while the state of M2 becomes closer to the state of R. So picking γ_{dec} is clearly a balance between getting $T_L \simeq T_{M1}$ for small γ_{dec} and $T_R \simeq T_{M2}$ for larger γ_{dec} .

III. CONCLUSION

We have studied three different heat-based circuits: a series configuration of diodes, a parallel configuration of diodes, and a diode bridge rectifier. The series configuration of diodes was found to result in an effective diode with similar rectification factors as for a single diode. The parallel configuration of

diodes was found to result in an effective diode with rectification factors similar to or larger than a single diode. Larger rectification factors were found for two qubit diodes of different anharmonicities. Finally, it was found that a heat-based diode bridge rectifier can be constructed similar to the full wave bridge rectifier in electronics. One output harmonic oscillator reaches the temperature of the hot bath, and for large anharmonicities, the other output harmonic oscillator reaches the temperature of the cold bath. The cold output only got cold when decoherence was included, and the ideal decoherence rate γ_{dec}/J was found to be $10^{-3} - 10^{-2}$. This is within the capabilities of current quantum technology platforms such as superconducting circuits [32], and trapped ions [33, 34].

IV. METHODS

In the main text, we studied the properties of the steady-state. However, due to the time-dependent Hamiltonian the steady state will not obey $\partial_t \hat{\rho} = 0$, instead the density matrix is evolved until the current converges. The upper part of the bridge rectifier has a time-independent Hamiltonian, and the steady state can be solved through diagonalization. The harmonic oscillator M1 is truncated to $N = 8$ states such that even the upper levels, which are kept, have negligible population. In Fig. 5(a), the forward and reverse bias currents are plotted as a function of time. To ensure that the current is allowed to converge, we use the average current

$$\mathcal{J}_{f/r,n} = \frac{1}{T_{\text{av}}} \int_{(n+1)T - T_{\text{av}}}^{(n+1)T} \mathcal{J}_{f/r}(t) dt,$$

where n determines for how long the density matrix is evolved, and we have picked $T = 5000J^{-1}$ and $T_{\text{av}} = 1000J^{-1}$. In Fig. 5(b), the average current $\mathcal{J}_{f/r,n}$ is plotted as a function of n . We say that the current is converged when

$$\frac{\mathcal{J}_{f/r,n} - \mathcal{J}_{f/r,n-1}}{\mathcal{J}_{f/r,n-1}} < 10^{-4},$$

and we set $\mathcal{J}_{f/r} = \mathcal{J}_{f/r,n}$. With this rule the current has converged for $n = 1$ and $n = 15$ for the forward and reverse bias currents, respectively, in Fig. 5(b).

V. ACKNOWLEDGEMENTS

The authors acknowledge funding from The Independent Research Fund Denmark DFF-FNU. The numerical results presented in this work were obtained at the Centre for Scientific Computing, Aarhus.

[1] C. A. Mack, Fifty years of moore's law, *IEEE Trans. Semicond. Manuf.* **24**, 202 (2011).

[2] I. Žutić, J. Fabian, and S. Das Sarma, Spintronics: Fundamentals and applications, *Rev. Mod. Phys.* **76**, 323 (2004).

- [3] S. Wolf, D. Awschalom, R. Buhrman, J. Daughton, S. Von Molnar, M. Roukes, A. Y. Chtchelkanova, and D. Treger, Spintronics: a spin-based electronics vision for the future, *Science* **294**, 1488 (2001).
- [4] K. Poulsen and N. T. Zinner, Giant magnetoresistance in boundary-driven spin chains, *Phys. Rev. Lett.* **126**, 077203 (2021).
- [5] N. Li, J. Ren, L. Wang, G. Zhang, P. Hänggi, and B. Li, Colloquium: Phononics: Manipulating heat flow with electronic analogs and beyond, *Rev. Mod. Phys.* **84**, 1045 (2012).
- [6] N. Roberts and D. Walker, A review of thermal rectification observations and models in solid materials, *Int. J. Therm. Sci.* **50**, 648 (2011).
- [7] H. T. Quan, Y.-x. Liu, C. P. Sun, and F. Nori, Quantum thermodynamic cycles and quantum heat engines, *Phys. Rev. E* **76**, 031105 (2007).
- [8] K. Ono, S. N. Shevchenko, T. Mori, S. Moriyama, and F. Nori, Analog of a quantum heat engine using a single-spin qubit, *Phys. Rev. Lett.* **125**, 166802 (2020).
- [9] L. Bresque, P. A. Camati, S. Rogers, K. Murch, A. N. Jordan, and A. Auffèves, Two-qubit engine fueled by entanglement and local measurements, *Phys. Rev. Lett.* **126**, 120605 (2021).
- [10] J. B. Brask, G. Haack, N. Brunner, and M. Huber, Autonomous quantum thermal machine for generating steady-state entanglement, *New Journal of Physics* **17**, 113029 (2015).
- [11] S. Lloyd, Quantum-mechanical maxwell's demon, *Phys. Rev. A* **56**, 3374 (1997).
- [12] C. Elouard, D. Herrera-Martí, B. Huard, and A. Auffèves, Extracting work from quantum measurement in maxwell's demon engines, *Phys. Rev. Lett.* **118**, 260603 (2017).
- [13] K. Poulsen, M. Majland, S. Lloyd, M. Kjaergaard, and N. T. Zinner, Quantum maxwell's demon assisted by non-markovian effects, *Phys. Rev. E* **105**, 044141 (2022).
- [14] J. V. Koski, V. F. Maisi, T. Sagawa, and J. P. Pekola, Experimental observation of the role of mutual information in the nonequilibrium dynamics of a Maxwell demon, *Phys. Rev. Lett.* **113**, 030601 (2014).
- [15] M. Naghiloo, J. J. Alonso, A. Romito, E. Lutz, and K. W. Murch, Information gain and loss for a quantum Maxwell's demon, *Phys. Rev. Lett.* **121**, 030604 (2018).
- [16] J. Senior, A. Gubaydullin, B. Karimi, J. T. Peltonen, J. Ankerhold, and J. P. Pekola, Heat rectification via a superconducting artificial atom, *Commun. Phys.* **3**, 40 (2020).
- [17] A. Ronzani, B. Karimi, J. Senior, Y.-C. Chang, J. T. Peltonen, C. Chen, and J. P. Pekola, Tunable photonic heat transport in a quantum heat valve, *Nat. Phys.* **14**, 991 (2018).
- [18] K. Joulain, J. Drevillon, Y. Ezzahri, and J. Ordóñez-Miranda, Quantum thermal transistor, *Phys. Rev. Lett.* **116**, 200601 (2016).
- [19] M. Majland, K. S. Christensen, and N. T. Zinner, Quantum thermal transistor in superconducting circuits, *Phys. Rev. B* **101**, 184510 (2020).
- [20] B.-q. Guo, T. Liu, and C.-s. Yu, Quantum thermal transistor based on qubit-qutrit coupling, *Phys. Rev. E* **98**, 022118 (2018).
- [21] K. Poulsen and N. T. Zinner, Dark state induced heat rectification, *arXiv:2203.12623* (2022).
- [22] A. Marcos-Vicioso, C. López-Jurado, M. Ruiz-García, and R. Sánchez, Thermal rectification with interacting electronic channels: Exploiting degeneracy, quantum superpositions, and interference, *Phys. Rev. B* **98**, 035414 (2018).
- [23] I. Díaz and R. Sánchez, The qutrit as a heat diode and circulator, *New J. Phys.* **23**, 125006 (2021).
- [24] A. Iorio, E. Strambini, G. Haack, M. Campisi, and F. Giazotto, Photonic heat rectification in a system of coupled qubits, *Phys. Rev. Appl.* **15**, 054050 (2021).
- [25] T. Werlang, M. A. Marchiori, M. F. Cornelio, and D. Valente, Optimal rectification in the ultrastrong coupling regime, *Phys. Rev. E* **89**, 062109 (2014).
- [26] D. Segal, Heat flow in nonlinear molecular junctions: Master equation analysis, *Phys. Rev. B* **73**, 205415 (2006).
- [27] K. Poulsen, A. C. Santos, L. B. Kristensen, and N. T. Zinner, Entanglement-enhanced quantum rectification, *Phys. Rev. A* **105**, 052605 (2022).
- [28] K. Pollak, Improvements in means for controlling or directing electric currents. (British patent 24398, Dec. 1886).
- [29] G. Lindblad, On the generators of quantum dynamical semi-groups, *Commun. Math. Phys.* **48**, 119 (1976).
- [30] H. Breuer and F. Petruccione, *The theory of open quantum systems* (Oxford University Press, Oxford, 2002).
- [31] K. Poulsen, A. C. Santos, and N. T. Zinner, Quantum wheatstone bridge, *Phys. Rev. Lett.* **128**, 240401 (2022).
- [32] M. Kjaergaard, M. E. Schwartz, J. Braumüller, P. Krantz, J. I.-J. Wang, S. Gustavsson, and W. D. Oliver, Superconducting qubits: Current state of play, *Annu. Rev. Condens. Matter Phys.* **11**, 369 (2020).
- [33] M. Johanning, A. F. Varón, and C. Wunderlich, Quantum simulations with cold trapped ions, *J. Phys. B* **42**, 154009 (2009).
- [34] H. Häffner, C. Roos, and R. Blatt, Quantum computing with trapped ions, *Phys. Rep.* **469**, 155 (2008).